Analytical formulae in fluid power, quo vadis in times of CFD and I4.0?

Zoufiné Lauer-Baré*, Erich Gaertig*, Johannes Krebs* and Christian Sleziona*

Hilite International, Simulation Department, Weberstraße 17, 72622 Nürtingen, Germany*
E-Mail: zoufine.lauer-bare@hilite.com

The aim of this contribution is to present up-to-date tables, which summarize the state-of-the-art relations for annular flow velocities, flow rates and flow forces in Newtonian, stationary incompressible Couette- and Poiseuille-flows, considering concentric and eccentric annuli together with limiting cases for small gaps. These analytical relations can then be applied to custom system simulation components and look-up tables for entire system simulations. Tailor-made simulation components (digital twins) containing analytical formulae are easily shared between customers and vendors, enhancing cross-entrepreneurial product optimization. All presented formulae are derived from the 3D Navier-Stokes equations and the high accuracy of the analytical formulae are validated with 3D CFD-simulations for selected representative cases.

Keywords: Eccentric annular flow, system simulation, digitalization, cross-entrepreneurial product optimization
Target audience: Design engineers, simulation engineers, system simulation software developers

1 Introduction

Computational power has increased significantly in the last couple of years and fluid dynamic problems can now be solved directly by numerically integrating the Navier-Stokes equations. However, when modelling fluid power systems such as hydraulic valves, transmission systems, artificial hearts or the human brain, a direct 3D-modelling of all relevant physical effects and operating points is still too difficult and time-consuming. In these situations, system simulation software is often used, which solves simplified 0D- and 1D-models. The various components utilized there are often based on analytical relationships between input and output quantities. In times of connectivity and I4.0, a cross-entrepreneurial product optimization realized e.g. by exchanging system simulation components (digital twins) is fundamental. Popular system simulation tools are for instance Simcenter Amesim, ANSYS Twin Builder, Dymola, DSHPlus, GT-SUITE or OpenModelica.

For reliable results, it is important that the appropriate analytical relationships are implemented in the system simulation software. However, in literature and software alike, these relationships may vary and it is not clear at all which versions are the appropriate ones. Depending on the edition of classical fluid power text books such as Matthies and Renius [15], Findeisen [4], Blackburn et al. [2] or Khaimovich [8] one can find different exponents or radii in the formulae for e.g. flow rates or fluid forces, which may or may not or depend on further parameters like eccentricity.

The analytical relations we focus on in this work are the flow rates and flow forces in concentric and eccentric annular flow domains. Annular flow between two cylinders is of interest when modelling electro-hydraulic valve systems, where the annular flow describes the internal leakage between bushing and spool or the fluid flow caused by electric actuation between armature and polecap. Another example, in this case related to hemodynamics, is the flow of cerebrospinal fluid in periarterial spaces (Tithoff et al. [24]). In all these applications, both the flow rates and forces that act on the inner ‘cylinder’ (armature, spool or penetrating artery in Figure **1**) are relevant (Lauer-Baré et al [13], Secomb [23]). In another application, Secomb and El-Kareh [22] showed a case where hemodynamic annular flow occurs in arteries due to aggregated red-cells that represent a moving ‘core’.

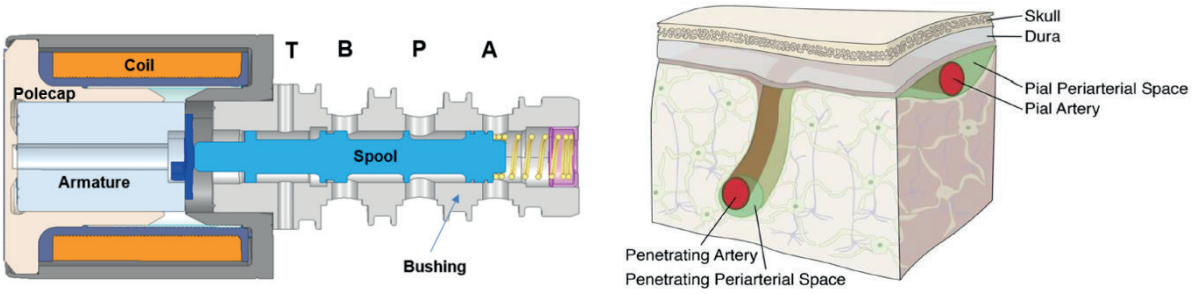

Figure 1: Annular flow applications; electrohydraulic valve from Hilite[1] (left) and arteries surrounded by periarterial spaces in the human brain (right, image taken from Tithoff et al. [24])

From the fluid mechanical perspective, the equations that govern the velocity distribution of oil or blood in the cases mentioned above are given by the Navier-Stokes equations. In many applications though it suffices to consider the related incompressible, steady state version. The flow rate and flow force formulae found in current literature vary between different authors and it is not clear at all which version is correct, when they apply and how they are related to the governing Navier-Stokes system.

The strategy to obtain correct flow forces and flow rates in this work consists in solving the corresponding Stokes problem analytically in a 2D annular domain (Figure **2**) for the axial fluid velocity and then compute flow forces and flow rates via analytical postprocessing. That is the main content of the following sections. In flows through annular domains, often the axial fluid velocity component dominates and as explained in Lauer-Baré et al [13], White [25], in this case the steady-state incompressible Navier-Stokes system can be simplified to obtain the steady-state Stokes equation.

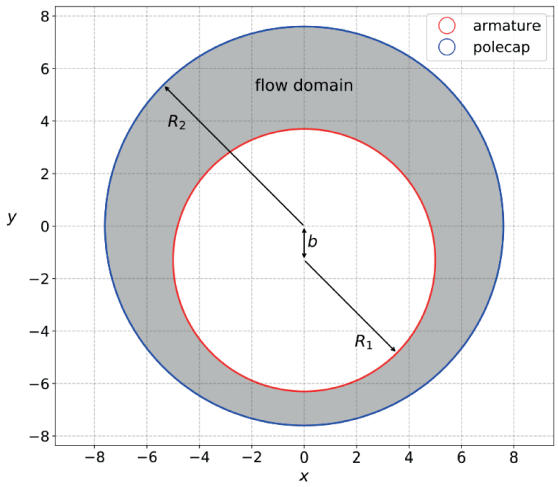

Figure 2: 2D annular flow domain obtained as cross-section of two eccentrically mounted cylinders (here armature and polecap are used, compare with left part of Figure **1***)*

The Stokes equation in annular domains as depicted in Figure **2** supplemented by boundary conditions for a moving inner cylinder reads as follows:

$$-\mu\Delta u = \frac{\Delta p}{l} \quad \text{for } R_1 < \sqrt{x^2 + (y+b)^2} \text{ and } \sqrt{x^2 + y^2} < R_2 \tag{1}$$

$$u(x,y) = 0 \quad \text{for } \sqrt{x^2 + y^2} = R_2$$

$$u(x,y) = u_A \quad \text{for } \sqrt{x^2 + (y+b)^2} = R_1$$

[1] https://www.hilite.com/en/company

Here, b is the absolute eccentricity and R_1, R_2 denote the radius of inner and outer cylinder respectively. The moving inner cylinder drags the fluid with it and leads to a fixed fluid velocity of u_A across its surface.

It is reminded that the system (1) describes Couette-flow when $\Delta p = 0$ and $u_A \neq 0$, Poiseuille-flow when $\Delta p \neq 0$ and $u_A = 0$ and Couette-Poiseuille flow when $\Delta p \neq 0$ and $u_A \neq 0$. Since (1) is a linear problem, Couette-Poiseuille flow can be obtained by superposing Couette- and Poiseuille-flow. l denotes the length of the cylinders, Δp the pressure drop and μ the dynamic viscosity of the fluid.

The ultimate aim of this contribution is to present up-to-date tables, which summarize the state-of-the-art of Newtonian, stationary, incompressible annular flow velocities, flow rates and flow forces that act on the surface of the inner cylinders (for example on armature, spool, or arteries). This includes Couette- and Poiseuille-flow, concentric and eccentric annuli as well as limiting cases for small gaps.

2 Previous Works and Methods

In order to solve (1) for the velocity and perform corresponding postprocessing, results from Piercy et al [20], White [25], Lauer-Baré et al. [13] and Lauer-Baré and Gaertig [14] are summarized and extended. The methods used for these kinds of problems in the state-of-the-art literature are briefly referenced as well.

In the concentric case, it is a standard approach to express the problem in radial coordinates (see e.g. White [25] or Landau and Lifshitz [11]) and to seek the velocity distribution in the form of

$$u(r) = c_1 \cdot r^2 + c_2 \cdot \ln r + c_3 \tag{2}$$

The eccentric case on the other hand is not as straightforward. There it is common to transform the eccentric annulus given in standard x-y Cartesian coordinates to a simpler domain with conformal mappings (see Lauer-Baré and Gaertig [14]), i.e. holomorphic functions in the complex plane. The map can be specified by using two new coordinates ξ, η, together with instructions on how to transform between these two systems via $w(x + iy) = \xi + i\eta$. The problem is then solved more easily in the new coordinates ξ, η in the simple domain (typically called the *w*-plane) and then transformed back to the original domain. One big advantage of conformal mappings is that they preserve harmonic functions. There is no trade-off between a simpler domain but a more complicated differential equation to solve; harmonic functions in one domain remain harmonic in the other domain as well. Piercy et al. [20] transformed an eccentric annulus to a rectangle in order to solve the corresponding Poiseuille-problem.

Recently, Lauer-Baré and Gaertig [14] extended Piercy's result to Couette-flow, too. Additionally, Lauer-Baré and Gaertig [14] solved the Couette-flow problem in an eccentric annulus by mapping the eccentric annulus to a concentric annulus[2] (*Figure* **3***a)*. Lauer-Baré and Gaertig [14] used slightly adapted transformations from Piercy et al. [20] and Brown and Churchill [3] (Figure **3***b*). With the abbreviation $z = x + iy$ the transformation to the concentric annulus reads as $w(x + iy) = (z + ia)/(az + i)$ and the conformal map to the rectangle is given by $w(x + iy) = 2 \cdot \arctan((z + \gamma i)/c)$; the constants are specified in the following sections.[3] A similar transformation as in Piercy et al [20] was used in Secomb and El-Kareh [22], where the velocity, flow rate and flow force of the eccentric Couette-flow are computed. Conformal mappings where also used recently with SymPy in the context of potential flow in Grm [5].

[2] https://www.youtube.com/watch?v=P5ybpjv2uDA

[3] For an animation showing the unfolding of an eccentric annulus to a rectangle, see https://github.com/zolabar/ConformalMappingSympy

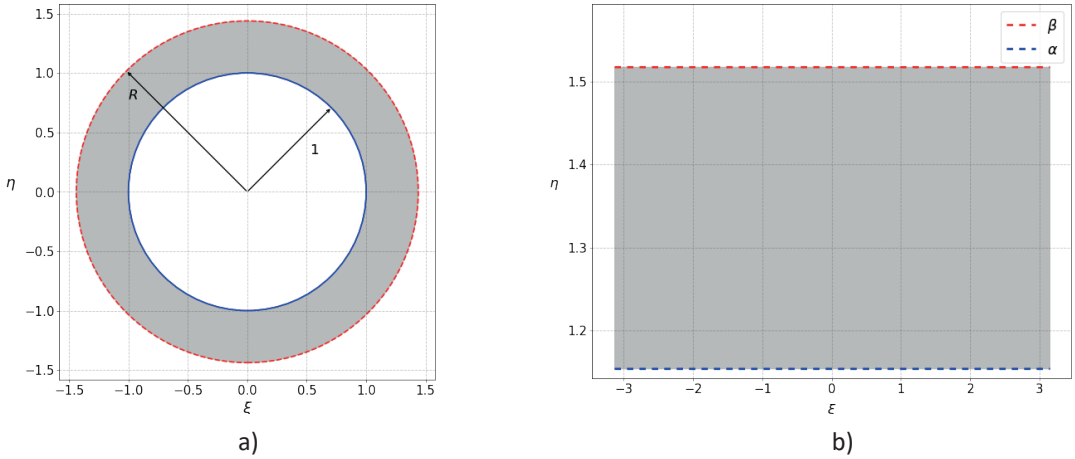

Figure 3: Flow domain in the w-plane after mapping the eccentric annulus of Figure **2** *to a concentric annulus (a) and to a rectangle (b); the colours indicate how inner and outer boundaries are mapped onto the simpler domain (compare with Figure* **2***)*

An implementation and 1D-visualization of Piercy's Poiseuille-flow velocity was presented by Kolitawong and Giacomin [9]. Lauer-Baré and Gaertig [14] visualized Piercy's Poiseuille-flow velocity and the corresponding Couette-flow velocity in 2D. As we know from Piercy et al. [20], once having found the velocity in such a way, the analytical computation of the flow force is easy. Not as simple as that however is the calculation of the corresponding flow rate, since this involves transforming integrals. In order to derive the limiting flow rates and flow forces for small gaps, Taylor expansions are used (see White [25] and Lauer-Baré et al [13]). Most of these expansions can be carried out with the help of the open-source computer algebra system (CAS) SymPy (Meurer et al [16] and Lauer-Baré and Gaertig [14])[4]. Finally, in order to approximate eccentric flow rates and flow forces by concentric flow rates and flow forces, Taylor expansions in the relative eccentricity are discussed. For selected cases, velocities and forces are compared to the corresponding results obtained from 3D Finite Volume Methods (using ANSYS CFX), which were used to solve the full set of Navier-Stokes equations.

3 Results

Before the velocities and their derived postprocessing expressions like flow rates and forces are stated, a comment on the existence and uniqueness of the velocities, i.e. solutions to (1) is in order. The system (1) has a unique solution, as proved by Ladyzhenskaya [10], hence all solution to (1) are identical when expressed in the same coordinates, once the boundary conditions are fixed. The different conformal mappings to the transformed w-plane, that by Ladyzhenskaya [10] all lead to the identical solution in the original z-plane, can be interactively visualized with the open-source software conformalMaps, e. g. via the Binder Project (see Project Jupyter et al. [7], Lauer-Baré and Aditya [12]).

3.1 Concentric annulus

3.1.1 Couette Flow

In the concentric case, that is $b = 0$ in (1) and Figure **2**, the velocity of the Couette-flow is given by

$$u_{CC}(r) = u_A \frac{\ln(r/R_2)}{\ln(R_1/R_2)} \tag{3}$$

The flow rate can be obtained by integration of the velocity distribution over the flow area

[4] https://github.com/zolabar/ConformalMappingSympy

$$Q_{CC} = \int_0^{2\pi} \int_{R_1}^{R_2} u_{CC}(r) r dr d\varphi = u_A \pi \cdot \left(\frac{\left({R_2}^2 - {R_1}^2 \right)}{2\, ln(R_2/R_1)} - {R_1}^2 \right) \tag{4}$$

The flow force can then be obtained by integrating the shear stress corresponding to (3) over the surface of the inner cylinder

$$F_{CC} = \int_0^{2\pi} \int_0^{l} \left(\mu r \frac{\partial}{\partial r} u_{CC}(r) \right)_{r=R_1} dx d\varphi = -u_A \frac{2\pi l \mu}{ln(R_2/R_1)} \tag{5}$$

A Taylor expansion of (4) in the gap $\delta = R_2 - R_1$ around $\delta = 0$ yields the flow rate for small gaps. The idea of these expansions is to compute all derivatives symbolically, either with SymPy or by hand, and to derive the limits, when the respective small parameter (gap or eccentricity) tends to zero. After substituting R_2 by $R_1 + \delta$ in (4) and considering Q_{CC} as a function of δ, the formula of the series for (4) is given by

$$Q_{CC} = Q_{CC}(\delta = 0) + \frac{\partial Q_{CC}(\delta = 0)}{\partial \delta} \delta + \frac{1}{2} \frac{\partial^2 Q_{CC}(\delta = 0)}{\partial \delta^2} \delta^2 + O(\delta^3) \tag{5.1}$$

The coefficients of this truncated power series are computed with SymPy and the final result is given by

$$Q_{CC} = u_A \pi R_1 \delta + \frac{u_A \pi R_1}{6} \delta^2 - \frac{\pi u_A}{180 \pi R_1} \delta^4 + O(\delta^5) \tag{6}$$

The constant, zeroth order term of (5.1) is zero and the leading term of (5.1) is the first order term $u_A \pi R_1 \delta$. Hence, (6) can be approximated for small gaps as

$$Q_{CC} \approx u_A \pi R_1 \delta \tag{7}$$

In addition, for small gaps a Taylor expansion of the denominator in (5) around $\delta = 0$ and a subsequent long division leads to a truncated Laurent series for the corresponding flow force

$$F_{CC} = -u_A 2\pi R_1 l \mu \delta^{-1} - u_A l \pi \mu + \frac{u_A l \pi \mu}{6 R_1} \delta + O(\delta^2) \tag{8}$$

Hence for small gaps this can be approximated by

$$F_{CC} \approx= -u_A 2\pi R_1 l \mu \delta^{-1} \tag{9}$$

3.1.2 Poiseuille Flow

In the concentric case, that is $b = 0$ in (1) and Figure **2**, the velocity of the Poiseuille-flow is given by

$$u_{PC}(r) = \frac{\Delta p}{4 \mu l} \left({R_2}^2 - r^2 - ({R_2}^2 - {R_1}^2) \frac{ln(R_2/r)}{ln(R_2/R_1)} \right) \tag{10}$$

The flow rate can be obtained by integration of (10) over the flow domain (Piercy et al [20] and White [25])

$$Q_{PC} = \int_0^{2\pi} \int_{R_1}^{R_2} u_{PC}(r) r dr d\varphi = \frac{\pi \cdot \Delta p}{8 \cdot \mu \cdot l} \left({R_2}^4 - {R_1}^4 - \frac{\left({R_2}^2 - {R_1}^2 \right)^2}{\ln(R_2/R_1)} \right) \tag{11}$$

The flow force can then be obtained by integration of the shear stress corresponding to (10) over the surface of the inner cylinder (see Bird et al. [1])

$$F_{PC} = \int_0^{2\pi} \int_0^{l} \left(\mu r \frac{\partial}{\partial r} u_{PC}(r) \right)_{r=R_1} dx d\varphi = -\pi \Delta p \left({R_1}^2 - \frac{(R_2^2 - R_1^2)}{2 \ln(R_2/R_1)} \right) \tag{12}$$

A Taylor expansion of (11) around $\delta = 0$ yields the flow rate for small gaps

$$Q_{PC} = \frac{\pi \cdot \Delta p \cdot R_1}{6 \cdot \mu \cdot l} \cdot \left(\delta^3 + \frac{\delta^4}{2 \cdot R_1} + \frac{\delta^5}{60 \cdot R_1^2} \right) + O(\delta^6) \tag{13}$$

Hence for small gaps it is

$$Q_{PC} \approx \frac{\pi \cdot \Delta p \cdot R_1}{6 \cdot \mu \cdot l} \cdot \delta^3 \tag{14}$$

Similarly, a Taylor expansion of (12) around $\delta = 0$ yields the flow rate for small gaps

$$F_{PC} = \Delta p \pi R_1 \delta + \frac{\Delta p \pi}{6} \delta^2 - \frac{\Delta p \pi}{180 \cdot R_1^2} \delta^4 + O(\delta^5) \tag{15}$$

Hence for small gaps it is

$$F_{PC} \approx \Delta p \pi R_1 \delta \tag{16}$$

3.2 Eccentric annulus

3.2.1 Couette Flow

In the eccentric case, that is $b > 0$ in (1) and Figure **2**, the velocity of the Couette-flow velocity can be obtained by solving the Stokes equation in the *w*-plane (see Lauer-Baré and Gaertig [14] for details). When the eccentric annulus is transformed into a rectangle (see right part of Figure **3**), as done by Piercy et al. [20] for the Poiseuille-flow, one can extend Piercy's result to Couette-flow as described by Secomb and El-Kareh [22], and the velocity is given by the simple relationship

$$u_{CE}(\xi, \eta) = u_A \frac{\eta - \alpha}{\beta - \alpha} \tag{17}$$

where

$$\xi = -\arctan_2(2cx, c^2 - x^2 - (\gamma + y)^2) \tag{18}$$

$$\eta = \frac{1}{2} \ln \left(\frac{x^2 + (y + \gamma + c)^2}{x^2 + (y + \gamma - c)^2} \right)$$

and where the various constants are defined by

$$c = \sqrt{G^2 - R_2^2}, \quad G = {}^1\!/_{2b} \cdot \left({R_2}^2 - {R_1}^2 + b^2 \right), \tag{19}$$

$$\alpha = {}^1\!/_2 \cdot \ln[(G + c)/(G - c)], \ \beta = {}^1\!/_2 \cdot \ln[(G - b + c)/(G - b - c)], \ \gamma = c \cdot \coth(\alpha)$$

Alternatively to Secomb and El-Kareh [22], the velocity can be expressed in a different way, when transforming the eccentric annulus into a concentric annulus (see left part of Figure **3** and Lauer-Baré and Gaertig [14] for details). Then, the velocity reads as

$$u_{CE}(\rho) = u_A \frac{\ln(\rho)}{\ln(R)} \tag{21}$$

where $\rho = \sqrt{\xi^2 + \eta^2}$ and

$$\xi = \frac{ax^2 + (R_2 + ay)(R_2 a + y)}{a^2 x^2 + (R_2 + ay)^2} \tag{22}$$

$$\eta = \frac{x\left(-R_2 - ay + a(R_2 a + y)\right)}{a^2 x^2 + (R_2 + ay)^2}$$

and the constants a and R are given by

$$a = \frac{R_2\left(\sqrt{\left(1-\left(-\frac{R_1}{R_2}+\frac{b}{R_2}\right)^2\right)\left(1-\left(\frac{R_1}{R_2}+\frac{b}{R_2}\right)^2\right)}+\left(-\frac{R_1}{R_2}+\frac{b}{R_2}\right)\left(\frac{R_1}{R_2}+\frac{b}{R_2}\right)+1\right)}{2b} \tag{23}$$

$$R = \frac{R_2\left(\sqrt{\left(1-\left(-\frac{R_1}{R_2}+\frac{b}{R_2}\right)^2\right)\left(1-\left(\frac{R_1}{R_2}+\frac{b}{R_2}\right)^2\right)}-\left(-\frac{R_1}{R_2}+\frac{b}{R_2}\right)\left(\frac{R_1}{R_2}+\frac{b}{R_2}\right)-1\right)}{2R_1}$$

As already briefly mentioned in the beginning of Section 3, by Ladyzhenska's [10] theorems the relations (17) and (21) lead to the identical solution when expressed in the same coordinate system, i.e. the original flow domain. The flow rate was obtained by Secomb and El-Kareh [22] and reads as

$$Q_{CE} = -\pi u_A\left({R_1}^2 - \frac{bc}{\beta-\alpha}\right) \tag{24}$$

The flow force can be obtained by integration in the w-plane. The force obtained from (17) reads as

$$F_{CE} = -2\pi\frac{u_A l\mu}{\beta-\alpha} \tag{25}$$

while the corresponding force obtained from (21) is given by

$$F_{CE} = -\frac{u_R 2\pi l\mu}{\ln(c_F \cdot R_2/R_1)} \tag{26}$$

Here the various constants are defined as

$$c_F = \frac{1}{2} - \frac{1}{2}c_1 c_2 + \frac{1}{2}\sqrt{(1-{c_1}^2)(1-{c_2}^2)}$$

$$c_1 = \frac{R_1}{R_2} + \frac{b}{R_2}$$

$$c_2 = -\frac{R_1}{R_2} + \frac{b}{R_2}$$

In the eccentric case both force formulae (25) and (26) are of course identical, however (26) has the advantage, that it is also defined for the concentric case ($b = 0$), therefore we recommend using that relation. As in the sections before, Taylor expansions can be carried out with respect to gap size and relative eccentricity. Combining these results from Lauer-Baré et al [13] and the flow rate (24) from Secomb and El-Kareh [22], one obtains

$$Q_{CE} \approx Q_{CC}(1 + a(\kappa)\varepsilon^2) \tag{27}$$

where $\kappa = R_1/R_2$ is the ratio of inner to outer radius and

$$a(\kappa) = -(1-\kappa)\frac{(1-\kappa^2) + \ln(\kappa)\,(1+\kappa^2)}{2\left(\kappa^2 + \frac{(1-\kappa^2)}{2\ln(\kappa)}\right)\ln^2(\kappa)\,(1+\kappa)}$$

For small gaps, this can be further simplified by combing a result from Lauer-Baré et al [13] and relation (7)

$$Q_{CE} \approx u_A \pi R_1 \delta\left(1 + \frac{(1-\kappa)}{6}\varepsilon^2\right) \tag{28}$$

3.2.2 Poiseuille Flow

In the eccentric case, that is $b > 0$ in (1) and Figure **2**, the velocity of the Poiseuille-flow reads as

$$u_{PE} = \frac{c^2 \Delta p}{4 l \mu}\left(\Psi - \frac{-\cos(\xi) + \cosh(\eta)}{\cos(\xi) + \cosh(\eta)}\right) \tag{29}$$

where ξ, η are the new coordinates from (18) and c is a constant from (19). Furthermore, Ψ is a harmonic function introduced by Piercy et al. [20] and is given by

$$\Psi = 4 \cdot \Psi_1 + 4 \cdot A \cdot \eta + 4 \cdot B \tag{30}$$

with

$$\Psi_1 = \sum_{k=1}^{\infty} \frac{(-1)^k (s_1 + s_2)\cos(k\xi)}{\sinh(k(\beta - \alpha))} \tag{31}$$

and

$$s_1 = e^{-k\beta}\sinh(k(\eta - \alpha))\coth(\beta) \tag{32}$$

$$s_2 = -e^{k\alpha}\sinh(k(\eta - \beta))\coth(\alpha)$$

as well as

$$A = \frac{\coth(\beta) - \coth(\alpha)}{2(\beta - \alpha)} \tag{33}$$

$$B = \frac{-\beta(1 - 2\coth(\beta)) + \alpha(1 - 2\coth(\alpha))}{4(\beta - \alpha)}$$

The formulae above are implemented and documented in interactive Jupyter notebooks that can be found on the public github repository ConformalMappingSympy[5]. The interested reader can use these notebooks to evaluate and visualize (29) and various other quantities.

The flow rate can again be obtained by integration of the velocity profile and is given by Piercy et al [20] via

$$Q_{PE} = \frac{\pi \cdot \Delta p}{8 \cdot \mu \cdot l}\left({R_2}^4 - {R_1}^4 - \frac{4b^2c^2}{\beta - \alpha} - 8b^2c^2 \sum_{k=1}^{\infty} \frac{k e^{(-k(\beta+\alpha))}}{\sinh(k(\beta - \alpha))}\right) \tag{34}$$

The flow force can then be calculated by integration in the *w*-plane (see Piercy et al. [20] for details) and the resulting force then reads as

$$F_{PE} = -\pi \Delta p \left({R_1}^2 - \frac{bc}{\beta - \alpha}\right) \tag{35}$$

The flow rate from (31) can be approximated by the concentric flow rate via (see Piercy et al. [20] for details)

$$Q_{PE} \approx Q_c(1 + 1.5\varepsilon^2) \tag{36}$$

where $\varepsilon = b/\delta$ denotes the relative eccentricity. Piercy et al. [20] already remarked that (36) is only valid for ratios $\kappa = R_1/R_2 > 0.6$. The authors of the current contribution think, that a factor that depends on the ratio κ and generalizes the constant term of 1.5 in relation (36) could be found by a Taylor expansion of (34) in the relative eccentricity ε around $\varepsilon = 0$, as done in Lauer-Baré et al. [13] for the corresponding flow forces. As far as we know, such a result for the flow forces has not been published yet. Using (14) for small gaps, (36) can be further simplified to

[5] https://github.com/zolabar/ConformalMappingSympy

$$Q_{PE} \approx \frac{\pi \cdot \Delta p \cdot R_1}{6 \cdot \mu \cdot l} \cdot \delta^3 (1 + 1.5\varepsilon^2) \tag{37}$$

As mentioned above, the eccentric flow force can be approximated by a series expansion and by using the concentric flow force. The result is given by

$$F_{PE} \approx F_{PC}(1 + a(\kappa)\varepsilon^2) \tag{38}$$

where

$$a(\kappa) = -(1-\kappa)\frac{(1-\kappa^2) + \ln(\kappa)\,(1+\kappa^2)}{2\left(\kappa^2 + \frac{(1-\kappa^2)}{2\ln(\kappa)}\right)\ln^2(\kappa)\,(1+\kappa)}$$

This formula was obtained via a Taylor expansion of (35) in the relative eccentricity ε around $\varepsilon = 0$. The corresponding flow force relation analogous to equation (36) for the flow rate is given by

$$F_{PE} \approx F_{PC}\left(1 + \frac{(1-\kappa)}{6}\varepsilon^2\right) \tag{39}$$

This relation is also valid for ratios $\kappa = R_1/R_2 > 0.6$, similar to relation (36). These results were obtained in Lauer-Baré et al. [13], too. Finally, in analogy to (37), (39) can be further simplified for small gaps to

$$F_{PE} \approx \Delta p \pi R_1 \delta \left(1 + \frac{(1-\kappa)}{6}\varepsilon^2\right) \tag{40}$$

3.2.3 Visualization of the analytically obtained fluid velocities

In order to highlight some qualitative effects on the velocity distribution, an example for a combined Couette-Poiseuille flow velocity distribution is shown in the following Figure **4**.

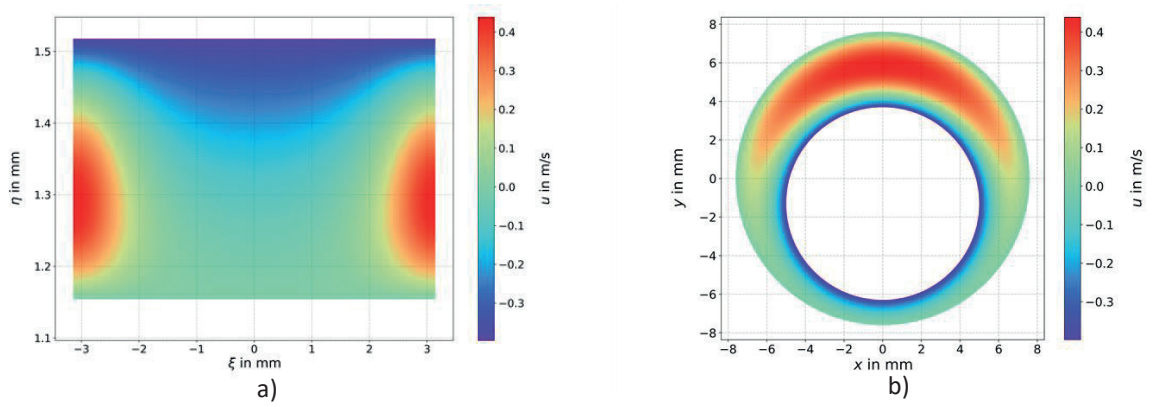

Figure 4: Example of a Couette-Poiseuille flow velocity profile by superposing (17) and (26) within a rectangle in the w-plane (a) and in the corresponding original eccentric annulus in the z-plane (b)

For this example, an outer radius of 7.6 mm, an inner radius of 5 mm, an eccentricity of 50%, a prescribed velocity of the inner cylinder of -0.4 m/s and a pressure drop of 5 Pa were used.[6] Further, an overlap of 1.55 mm and a viscosity of 10 mPa·s is used. One clearly sees, that the boundary conditions are satisfied. On the inner boundary of the eccentric annulus (Figure **4***b*) the velocity is non-zero and on the outer boundary it vanishes. Furthermore, in the interior the fluid disproportionally pours through the large gap, as already remarked in Piercy et al [20] and White [25]. The same behaviour is seen in Figure **4***a* in the equivalent rectangle in the *w*-plane. The boundary

[6] Replicable at https://mybinder.org/ with https://github.com/zolabar/ConformalMappingSympy

correspondence is illustrated in Figure **2** and Figure **3***b*, i.e. the top of the rectangle corresponds to the inner boundary of the annulus and the bottom of the rectangle corresponds to the outer boundary of the annulus.

3.2.4 CFD results

The following diagrams show the high quality of the analytical approximations (velocity and flow force) when compared to CFD-results.

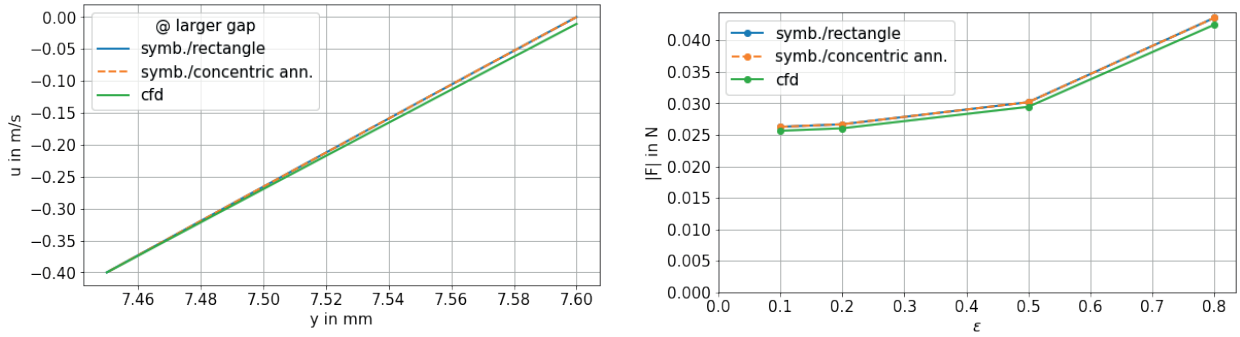

Figure 5: Eccentric Couette flow velocity ($\varepsilon = 0.5$) across the large gap of the annulus (left) and flow force over relative eccentricity (right), 3D numerical and 2D analytical results (from Lauer-Baré and Gaertig [14])

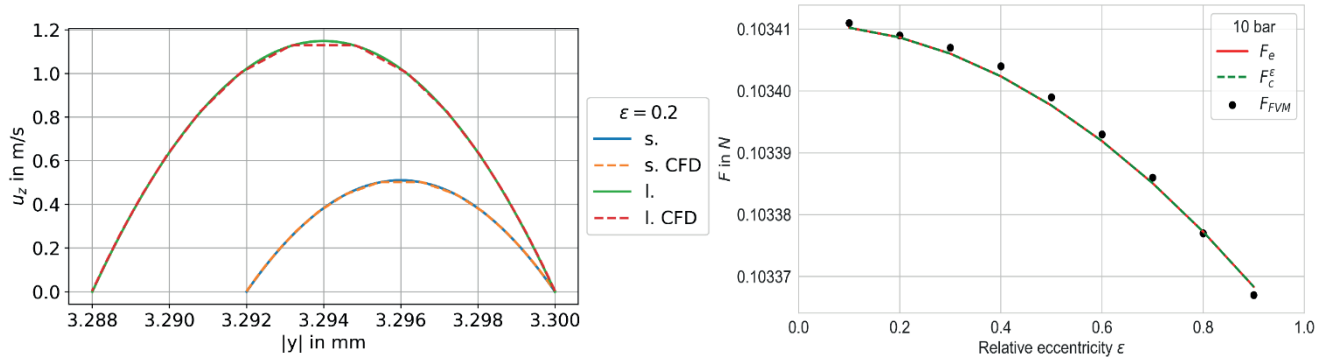

Figure 6: Eccentric Poiseuille flow velocity ($\varepsilon = 0.2$) across larger and smaller gap of the annulus (left) and flow force over relative eccentricity, 3D numerical and 2D analytical results

Figure **5** shows eccentric Couette flow velocity (left) across the large gap for an eccentricity of $\varepsilon = 0.5$ and flow force over relative eccentricity (right); for more details see Lauer-Baré and Gaertig [14]). Figure **6** shows corresponding graphs for eccentric Poiseuille flow. Figure **6** (left) shows Poiseuille velocities across the small and large gap, that correspond to an eccentricity of $\varepsilon = 0.2$ in Figure **6** (right). These results and the numerical details are more thoroughly discussed in Lauer-Baré et al. [13]. One can see, that eccentricity reduces the absolute value of the flow force in case of Poiseuille-flow (Figure **6** (right)), while in the case of Couette-flow, the flow force is increased by eccentricity (Figure **5** (right)). It is also remarked, that in Poiseuille-flow the flow force acts in flow direction while in Couette-flow the flow force acts against the direction of the fluid flow. The high quality of the analytical solutions for the cross-sectional Stokes problem is due to the fact, that in the considered cases the axial component of the velocity is so dominant that the contribution of the nonlinear convective terms in the original Navier-Stokes equations is irrelevant (Lauer-Baré et al. [13]). Therefore, the 3D Navier-Stokes equations are approximated sufficiently well by the 2D Stokes equation (1). In Lauer-Baré et al. [13] it is conjectured, that a relevant a-priori indicator for the suitability of the Stokes equation is the ratio δ/l. The smaller this ratio, the more axial the flow and hence the better the Navier-Stokes system is approximated by the Stokes equation. In Figure **5** this ratio is 0.008 and in Figure **6** it is 0.026. However, as far as the authors know a rigorous study of the influence of the parameter δ/l in annular flow has not yet been carried out in the state-of-the-art literature. As suggested in

Lauer-Baré et al. [13], a proper analysis of the parameter δ/l using asymptotic expansions as in Panasenko and Pileckas [17] could be the content of future work.

3.3 Summary

This section contains the main message and result of this contribution. A tabularized systematic overview on analytical approximations of annular flow velocities, flow rates and flow forces for concentric and eccentric Couette- and Poiseuille-flow. The content of the following tables refers to the corresponding equations of the previous sections. Table **1** lists the available formulae for the velocities, Table **2** lists the available formulae for the flow rates and Table **3** lists the available formulae for the flow forces.

Velocity	**Concentric**	**Eccentric**
Couette	(3)	(17) or (21)
Poiseuille	(10)	(29)

Table 1: Annular flow velocities

Flow rate	**Concentric**	**Eccentric**	**Concentric and small gap**	**Eccentric and small gap**
Couette	(4)	(24)	(7)	(28)
Poiseuille	(11)	(33)	(14)	(37)

Table 2: Annular flow rates

Flow force	**Concentric**	**Eccentric**	**Concentric and small gap**	**Eccentric and small gap**
Couette	(5)	(25) or (26)	(9)	Not available
Poiseuille	(12)	(35)	(16)	(40)

Table 3: Annular flow forces

Before closing this article with discussion and conclusions, some comments are in order. In our tables the approximation of the eccentric Couette-flow force by the concentric flow force is missing. This is due to fact, that the flow force formula (26) is defined for the concentric case as well, hence there is no need for a separate approximation of the eccentric flow force by the corresponding concentric contribution as in (38). We also want to stress, that the factor “1.5” in (37) (and in (36) as well) is not obtained by a Taylor expansion in the relative eccentricity and the general expression, corresponding to the factor $a(\kappa)$ in (27) or (38), is still unknown to fluid power science. Finally, we want to remark that in the case of Poiseuille-flow eccentricity increases the magnitude of the flow rate and reduces the magnitude of the flow force, while in the case of Couette-flow it is vice versa.

4 Discussion and Conclusion

This contribution showed that Newtonian, stationary, incompressible annular flow can be described in high quality by the 2D-Stokes equation, formulated in the cross section, when the ratio of annular gap to cylinder length is negligible. However, when instead of fluids like oil, water or blood, low-viscosity gases like hydrogen are considered (e.g. for application in FCEVs), more differentiated a priori estimates will be necessary. In these cases,

it could be possible to combine the ratio of annular gap to cylinder length with the viscosity of the gas into one single formula.

Well-known and recently presented analytical solutions of the Stokes equation are presented in a systematic way, considering concentric and eccentric annuli for Couette- and Poiseuille-flow. Further, the corresponding flow rates and flow forces are presented. The flow rates and forces are also derived for the limiting case of small gaps. Additionally, some of the flow rates and flow forces are approximated by their concentric counterparts, which are corrected by an auxiliary term in the squared relative eccentricity. The high quality of these analytical approximations was illustrated via comparisons with corresponding results obtained from a numerical solution of the 3D Navier-Stokes equations, computed with the commercial Finite Volume Method software ANSYS CFX. The obtained results can be used to generate look-up-tables for system simulations of fluid power systems by simulation engineers or can also be implemented directly into the system simulation software by developers. Further, design engineers can use these formulae during the design process, prior to detailed simulations. Finally, these results may be extended to non-steady cases following Pasquini et al [14] and Pasquini [15], to thermal flow following Shah and London [21] or to non-Newtonian fluids, as in Kolitawong and Giacomin [9].

The increasing demand on battery cooling fluid power applications may foster the interest in annular flow that considers thermal effects as presented in Shah and London [21]. One example of such systems are thermal expansion valves[7] as developed by Hilite International.

The quality and use cases of the presented analytical formulae, as well as the indicated perspectives, show that analytical formulae are still relevant and useful in times of wide use of numerical and machine learning techniques. Further, the implementation and visualization of analytical approaches gets easier with the use of open-source or commercial CAS such as SymPy, Maple, Mathematica or Singular (see Hauck et al. [6]), combined with interactive plotting possibilities, as for example provided by the open source Python package Plotly. The authors thus conclude, that analytical approaches also have a great potential for the future.

Nomenclature

Variable	*Description*	*Unit*
u	Axial flow velocity	[m/s]
u_{CC}	Axial flow velocity of concentric Couette flow	[m/s]
u_{CE}	Axial flow velocity of eccentric Couette flow	[m/s]
u_{PC}	Axial flow velocity of concentric Poiseuille flow	[m/s]
u_{PE}	Axial flow velocity of eccentric Poiseuille flow	[m/s]
Q_{CC}	Flow rate of concentric Couette flow	[l/min]
Q_{CE}	Flow rate of eccentric Couette flow	[l/min]
Q_{PC}	Flow rate of concentric Poiseuille flow	[l/min]
Q_{PE}	Flow rate of eccentric Poiseuille flow	[l/min]
F_{CC}	Flow force acting on inner cylinder in concentric Couette flow	[N]
F_{CE}	Flow force acting on inner cylinder in eccentric Couette flow	[N]
F_{PC}	Flow force acting on inner cylinder in concentric Poiseuille flow	[N]

[7] https://www.hilite.com/en/products/thermal-management/components-for-coolants

F_{PE}	Flow force acting on inner cylinder in eccentric Poiseuille flow	[N]
R_1	Denotes the radius of the inner cylinder	[mm]
R_2	Denotes the radius of the outer cylinder	[mm]
$\delta = R_2\text{-}R_1$	Denotes the annular gap or clearance between the cylinders	[mm]
b	Denotes the absolute eccentricity (shift) of the inner cylinder	[mm]
$\varepsilon = b/\delta$	Denotes the relative eccentricity of the inner cylinder	[-]
$\kappa = R_1/R_2$	Denotes the ratio of inner to outer radius	[-]
l	Denotes the length of the cylinders	[mm]
Δp	Denotes the pressure drop	[bar]
μ	Denotes the dynamic viscosity of the fluid	[mPa·s]

References

[1] Bird, B., Steward W., Lightfoot, E., Transport Phenomena, 2nd Edition, John Wiley & Sons, Inc., 2002.

[2] Blackburn, J., ed. Fluid power control. Mit Press, 1969.

[3] Brown JW, Churchill RV. Complex variables and applications, McGraw-Hill, NY; 2009, ISBN 978-0-0733-8317-0

[4] Findeisen D. Ölhydraulik: Handbuch für die hydrostatische Leistungsübertragung in der Fluidtechnik. Springer-verlag; 1994.

[5] Grm, A., Ships Added Mass Effect on a Flexible Mooring Dolphin in Berthing Manoeuvre. J. Mar. Sci. Eng. 2021, 9, 108. https://doi.org/10.3390/jmse9020108

[6] Hauck M, Orlik J, Levandovskyy V, Lykhachova O. Symbolic homogenization and structure optimization for a periodically perforated cylindrical shell. ZAMM, 2021.

[7] Project Jupyter et al., "Binder 2.0 - Reproducible, Interactive, Sharable Environments for Science at Scale." Proceedings of the 17th Python in Science Conference. 2018. doi://10.25080/Majora-4af1f417-011

[8] Khaimovich, E. M., Hydraulic control of machine tools. Pergamon Press, 1965, Oxford.

[9] Kolitawong C, Giacomin AJ. Axial flow between eccentric cylinders. Polymer-Plastics Technology and Engineering. 40(3):363-84, 2001 , DOI: 10.1081/PPT-100000254

[10] Ladyzhenskaya OA. The mathematical theory of viscous incompressible flow, Martino Publishing; 2014, ISBN 978-1-6142-7671-5

[11] Landau LD, Lifshitz EM. Fluid Mechanics, Pergamon Press, NY;1987, https://doi.org/10.1016/C2013-0-03799-1

[12] Lauer-Baré Z. and Aditya. Conformal-Maps: Code for interactive conformal mapping with python and jupyter notebook (v1.0.1). Zenodo. 2021. https://doi.org/10.5281/zenodo.5717868

[13] Lauer-Baré Z., Gaertig E., Krebs J., Arndt C., Sleziona A., Gensel A., A note on leakage jet forces: Application in the modelling of digital twins of hydraulic valves, International Journal of Fluid Power, 2021, Vol. 22 (1), 113–146. DOI: 10.13052/ijfp1439-9776.2214

[14] Lauer-Baré Z. and Gaertig E., Conformal Mappings with SymPy: Towards Python-driven Analytical Modeling in Physics. Lauer-Baré, Z. & Gaertig, E. In Agarwal, M., Calloway, C., Niederhut, D., & Shupe, D., editors, Proceedings of the 20th Python in Science Conference, pages 85 - 93, 2021. DOI: 10.25080/majora-1b6fd038-00b

[15] Matthies HJ, Renius KT. Einführung in die Ölhydraulik. Stuttgart: Teubner; 1984.

[16] Meurer A, Smith CP, Paprocki M, Certík O, Kirpichev SB, Rocklin M, Kumar A, Ivanov S, Moore JK, Singh S, Rathnayake T. SymPy: symbolic computing in Python, PeerJ Computer Science; 2017, https://doi.org/10.7717/peerj-cs.103

[17] Panasenko, G., Pileckas, K., Asymptotic analysis of the nonsteady viscous flow with a given flow rate in a thin pipe. Applicable Analysis, 91(3), 559-574, 2012.

[18] Pasquini E, Baum H, Murrenhoff H. Pressure Loss in Unsteady Annular Channel Flow. Universitätsbibliothek der RWTH Aachen; 2018.

[19] Pasquini E. G. Eindimensionale Berechnung instationärer Ringspaltströmungen mit thermofluiddynamischer Betrachtung. Reihe Fluidtechnik, RWTH Aachen, 2020.

[20] Piercy, N.A.V., Hooper, D.Sc., M.S. & Winny Ph.D., H.F., LIII. Viscous flow through pipes with cores, The London, Edinburgh, and Dublin Philosophical Magazine and Journal of Science, 1933.

[21] Shah, R. K., and London, A. L., Laminar Flow Forced Convection in Ducts, Advances in Heat Transfer, 1978.

[22] Secomb TW, El-Kareh AW. A model for motion and sedimentation of cylindrical red-cell aggregates during slow blood flow in narrow horizontal tubes. Journal of biomechanical engineering. 1994 Aug 1;116(3):243-9.

[23] Secomb TW. Hemodynamics. Comprehensive physiology. 2016;6(2):975.

[24] Tithof J, Kelley DH, Mestre H, Nedergaard M, Thomas JH. *Hydraulic resistance of periarterial spaces in the brain*. Fluids and Barriers of the CNS. 2019 Dec; 16(1):1-3.

[25] White, F. M., Viscous fluid flow. Vol. 3. McGraw-Hill, 2006, New York.